(red) pmoles of *PNKP-siRNA* (upper panel). PNKP levels normalized to β-actin are shown in the lower panel.
(TIF)

S11 Fig. Depletion of PNKP in SH-SY5Y cells activates the DNA damage response. **(A)** SH-SY5Y cells were transfected with plasmids expressing *PNKP-shRNAmir or control-shRNAmir* and the transfected cells analyzed by immunostaining with anti-P-53BP1-S1778 antibody (red); 53BP1 foci are shown by arrows. **(B)** Relative number of 53BP1 foci in SH-SY5Y cells transfected with plasmids encoding *control-shRNAmir* (upper panel) vs. *PNKP-shRNAmir* (lower panel). The data represent mean ± SD, n = 100, ***p = 0.001 in B and D. **(C)** SH-SY5Y cells were transfected with plasmids expressing either *PNKP-shRNAmir* or *control-shRNAmir* and the cells analyzed by immunostaining with anti-γH2AX-S139 antibody (red); γH2AX foci are shown by arrows. **(D)** Relative number of P-γH2AX foci in SH-SY5Y cells transfected with plasmids expressing either *control-shRNAmir* or *PNKP-shRNAmir*.
(TIF)

S12 Fig. Depletion of PNKP in cells activates the DNA damage-response pathway. **(A)** SH-SY5Y cells were transfected with 0, 2, 4 and 8 μg (lanes 1 to 4) of plasmid DNA expressing *PNKP-shRNAmir*; 48 hours post-transfection the cells were harvested and their lysates analyzed by Western blotting to determine PNKP, ATM-S1981, total ATM, γH2AX-S139, total H2AX, Chk2-T68 and total Chk2 levels; β-actin was used as loading control in A and C. **(B)** Relative levels of ATM-S1981, γH2AX-S139, Chk2-T68 with respect to the corresponding total protein in SH-SY5Y cells transfected with plasmid expressing *PNKP-shRNAmir*. Cells were transfected with 0 (grey bar), 2 (black bar), 4 (blue) and 8 μg (red) of plasmid expressing *PNKP-shRNAmir* (n = 3, data represent mean ± SD; *** = $p < 0.001$ in B and D). **(C)** SH-SY5Y cells were transfected with 0, 2, 4 and 8 μg (lanes 1 to 4) of plasmid DNA expressing *control-shRNAmir*; 48 hours post- transfections the cells were harvested and their lysates analyzed by Western blotting as in A. **(D)** Relative levels of ATM-S1981, γH2AX-S139, Chk2-T68 with respect to the corresponding total protein in SH-SY5Y cells transfected with plasmid expressing *control-shRNAmir*.
(TIF)

S13 Fig. Mutant ATXN3 activates the DNA damage-response pathway in a redox-independent fashion. **(A)** SH-SY5Y cells were differentiated, incubated with N-acetyl cysteine, and the expression of ATXN3-Q84 induced. Cells were harvested 0, 3, 6 and 12 days after induction (lanes 1 to 4), and their lysates analyzed by Western blotting to detect ATM-S1981, total ATM, γH2AX-S139 and total H2AX levels; β-actin was used as a loading control in A and C. **(B)** Relative levels of ATM-S1981 and γH2AX-S139 with respect to the corresponding total protein determined in the Western blots described in A. Cells were harvested after 0 (grey), 3 (black), 6 (blue) and 12 (red) days of ATXN3-Q84 expression in B and D; n = 3; data represent mean ± SD, *** = $p < 0.001$ in B and D. **(C)** Expression of ATXN3-Q84 was induced in SH-SY5Y cells overexpressing the antioxidant enzyme catalase; cell lysates were analyzed as in A. **(D)** Relative levels of ATM-S1981 and P-γH2AX-S139 with respect to the corresponding total protein were determined in Western blots described in C.
(TIF)

S14 Fig. Pharmacological inhibition of the ATM→p53 pathway ameliorates ATXN3-Q84-mediated caspase-3 activation. **(A)** Caspase-3 activities in SH-SY5Y cells expressing ATXN3-Q84 measured before and after treatment with ATM inhibitor Ku55933. **(B)** Caspase-3 activities in SH-SY5Y cells expressing ATXN3-Q28 and ATXN3-Q84 were measured before and after treatment with the p53 inhibitor Pifithrin-α. Caspase-3 activities are

expressed as percentage change normalized to control, and data represent means ± SD; (n = 3; *** = $p < 0.001$ in A and B).
(TIF)

S15 Fig. Mutant ATXN3 activates the c-Abl→PKCδ pathway. **(A)** Relative levels of c-Abl-T735, PKCδ-T311 and cleaved caspase-3 (caspase-3-C) with respect to the corresponding total protein in SH-SY5Y cells expressing ATXN3-Q84 (n = 3; data represents mean ± SD, *** = $p < 0.001$ in A to F). Cells were harvested after 0 (grey), 3 (black), 6 (blue) and 12 (red) days of ATXN3-Q84 expression in A and B. **(B)** Relative c-Abl-T735 and PKCδ-T311 levels in SH-SY5Y cells expressing ATXN3-Q84 and pre-treated with Ku55933. **(C)** Relative γH2AX-S139, c-Abl-T735, PKCδ-T311, and cleaved caspase-3 levels with respect to total protein in SH-SY5Y cells transfected with 0 (grey), 50 (black), 100 (blue) and 200 (red) pmoles of *PNKP-siRNA*. **(D)** Relative γH2AX-S139, c-Abl-T735, PKCδ-T311, and cleaved caspase-3 levels in SH-SY5Y cells transfected with 0 (grey), 50 (black), 100 (blue) and 200 (red) pmoles of *control-siRNA*. **(E)** Relative PKCδ-T311 with respect to total PKCδ in cells pre-treated with STI-571 and expressing ATXN3-Q84. Cells were harvested after 0 (grey), 3 (black), 6 (blue) and 12 (red) of expression. **(F)** Relative PKCδ-T311 with respect to total PKCδ in cells pre-treated with STI-571 and transfected with 0 (grey), 50 (black), 100 (blue) and 200 (red) pmoles of *PNKP-siRNA*.
(TIF)

S16 Fig. Mutant ATXN3 activates the c-Abl→PKCδ pathway via activating ATM. **(A)** SH-SY5Y cells were differentiated, incubated with Ku55933, transfected with 0, 50, 100 and 200 pmoles of *PNKP-siRNA* (lanes 1 to 4), and cell lysates analyzed by Western blotting to determine PNKP, γH2AX-S139, total H2AX, c-Abl-T735, total c-Abl, PKCδ-T311, total PKCδ, Caspase-3 (cleaved), caspase-3 (full-length); β-actin was used as loading control. **(B)** Relative levels of γH2AX-S139, c-Abl-T735, PKCδ-T311, cleaved caspase-3 with respect to the corresponding total protein in cells pre-treated with Ku55399 and transfected with 0 (grey), 50 (black), 100 (blue) and 200 (red) pmoles of *PNKP-siRNA*. PNKP levels were normalized to β-actin. Data represents mean ± SD, n = 3, *** = $p < 0.001$.
(TIF)

S17 Fig. Depletion of *PNKP* facilitates nuclear translocation of PKCδ. **(A)** SH-SY5Y cells were transfected with *PNKP-* or *control-siRNA* and the transfected cells were immunostained with anti-PKCδ antibody (green). The subcellular distribution of PKCδ was assessed by confocal microscopy; nuclei were stained with DAPI. **(B)** Nuclear and cytosolic protein fractions were isolated from SH-SY5Y cells transfected with *PNKP-* or *control-siRNA* and analyzed by Western blotting with anti-PKCδ antibody to determine the relative nuclear/cytosolic abundance of PKCδ; GAPDH and hnRNPC1 were used as cytosolic and nuclear markers, respectively. **(C)** Relative levels of PKCδ in cytosolic and nuclear protein fractions in cells transfected with *PNKP-siRNA* vs. *control-siRNA*. Data represents mean ± SD (n = 4; *** = $p < 0.001$)
(TIF)

S18 Fig. SCA3 transgenic mouse brain sections show increased nuclear PKCδ levels. Brain sections from the SCA3 transgenic mouse expressing mutant ATXN3-Q135 (CMVMJD135 mice) and control mouse were analyzed by immunostaining with anti-PKCδ antibody (red) to assess the sub-cellular distribution of PKCδ. Cytosolic presence of PKCδ in the control mouse brain sections are shown by arrowhead, and nuclear PKCδ in the transgenic mouse brain sections is shown by arrows; nuclei were stained with DAPI
(TIF)

S19 Fig. Mutant ATXN3 activates pro-apoptotic pathway by activating c-Abl kinase pathway. **(A)** Caspase-3 activities in SH-SY5Y cells expressing ATXN3-Q28 and ATXN3-Q84, and expressing ATXN3-Q28 and ATXN3-Q84 in the presence of STI-571; caspase-3 activities are expressed as percentage change normalized to control. Data represent means ± SD; (n = 3; *** = $p < 0.001$). **(B)** Caspase-3 activities in SH-SY5Y cells transfected with *PNKP-* or *control-siRNA*, and in SH-SY5Y cells pre-treated with the c-Abl inhibitor STI-571 and transfected with *PNKP-siRNA*; caspase-3 activities are expressed as percentage change normalized to control. Data represent means ± SD (n = 3; *** = $p < 0.001$).
(TIF)

Acknowledgments

We acknowledge the generosity of Dr. Henry Paulson for the gift of pEGP-ATXN3 clones, Dr. Jean Zhao for PNKP cDNA clone and Chang-Deng Hu for the bimolecular fluorescence (Bi-FC) plasmids. We also acknowledge Dr. Jean-Paul Vonsattel at the New York Brain Bank (NYBB), Columbia University for the brain tissue samples. We sincerely thank Dr. David Konkel for critically editing this manuscript.

Author Contributions

Conceived and designed the experiments: YL PSS TKH TA. Performed the experiments: RG YL XF SC HLZ ASF AC APH. Analyzed the data: PSS TKH TA ASF PM. Contributed reagents/materials/analysis tools: AHK TA TM SC. Wrote the paper: PSS TKH TA PM.

References

1. Kawaguchi Y, Okamoto T, Taniwaki M, Aizawa M, Inoue M et al, (1994) CAG expansion in a novel gene for Machado-Joseph disease at chromosome 14q32.1, Nat Genet, 8, 221–228. doi: 10.1038/ng1194-221 PMID: 7874163
2. Zoghbi HY, Orr HT (2000) Glutamine repeats and neurodegeneration. Ann Rev Neurosci, 23, 213–247. doi: 10.1146/annurev.neuro.23.1.217
3. Kobayashi T, Kakizuka A (2003) Molecular analysis of Machado-Joseph disease, Cytogenetic and Genome Res, 100, 261–275. doi: 10.1159/000072862
4. Rosenberg RN (1992) Machado-Joseph disease: an autosomal dominant system degeneration. Mov Disord, 3, 193–203. doi: 10.1002/mds.870070302
5. Takiyama Y, Oyanagi S, Kawashima S, Sakamoto H, Saito K et al, (1994) A clinical and pathologic study of a large Japanese family with Machado-Joseph disease tightly linked to the DNA markers on chromosome 14q, Neurology, 44, 1302–1308. doi: 10.1212/WNL.44.7.1302 PMID: 8035935
6. Durr A, Stevanin G, Cancel G, Duyckaerts C, Abbas N et al, (1996) Spinocerebellar ataxia 3 and Machado-Joseph disease: clinical, molecular and neuropathological features, Ann Neurol, 39, 490–499. doi: 10.1002/ana.410390411 PMID: 8619527
7. Klockgether T, Skalej M, Wedekind D, Luft AR, Welte D et al, (1998) Autosomal dominant cerebellar ataxia type 1: MRI-based volumetry of posterior fossa structures and basal ganglia in spinocerebellar ataxia type 1, 2 and 3, Brain, 121, 1687–1693. doi: 10.1093/brain/121.9.1687 PMID: 9762957
8. Di Prospero NA, Fishbeck KH (2005) Therapeutic development for triplet repeat expansion diseases, Nat Rev Genet, 6, 756–765. doi: 10.1038/nrg1690 PMID: 16205715
9. Costa MD and Paulson HL (2012) Toward understanding Machado-Joseph disease, Progress in Neurobiol, 97, 239–257. doi: 10.1016/j.pneurobio.2011.11.006
10. Winborn BJ, Travis SM, Todi SV, Scaglione KM, Xu P et al, (2008) The deubiquitinating enzyme ataxn-3, a polyglutamine disease protein, edits Lys63 linkages in mixed linkage ubiquitin chains, J Biol Chem, 283, 26436–43. doi: 10.1074/jbc.M803692200 PMID: 18599482
11. Todi SV, Scaglione KM, Blount JR, Basrur V, Conlon KP et al, (2010) Activity and cellular functions of the deubiquitinating enzyme and polyglutamine disease peotein ataxin-3 are regulated by ubiquitination at lysine 117, J Biol Chem, 285, 39303–39313. doi: 10.1074/jbc.M110.181610 PMID: 20943656

12. Matos CA, de Macedo-Ribeiro S, Carvalho AL (2011) Polyglutamine diseases: the special case of ataxin-3 and Machado Joseph disease, Prog Neurobiol, 95, 26–48. doi: 10.1016/j.pneurobio.2011.06.007 PMID: 21740957

13. Schmitt I, Linden M, Khazneh H, Evert BO, Breuer P et al, (2007) Inactivation of mouse Atxn3 (ataxin-3) gene increases protein ubiquitination, Biochem Biophy Res Commun, 362, 734–739. doi: 10.1016/j.bbrc.2007.08.062

14. Rodriguez-Lebron E, doCamro Costa M, Luna-Cancalon K, Peron TM, Fischer S et al, (2013): Silencing mutant ATXN3 expression resolves molecular phenotypes in SCA3 transgenic mice, Mol Therapy, 21, 1909–1918. doi: 10.1038/mt.2013.152

15. Chou A-H, Yeh T-H, Kuo Y-L, Kao Y-C, Jou M-J et al, (2006) Polyglutamine-expanded ataxin-3 activates mitochondrial apoptotic pathway by upregulating BAX and downregulating Bcl-XL, Neurobiol Dis, 21, 333–345. doi: 10.1016/j.nbd.2005.07.011 PMID: 16112867

16. Chou A-H, Lin A-C, Hong K-Y, Hu S-H, Chen Y-L et al, (2011) p53 activation mediates polyglutamine-expanded ataxin-3 upregulation of Bax expression in cerebellar and pontine nuclei neurons, Neurochem Int, 58, 145–152. doi: 10.1016/j.neuint.2010.11.005 PMID: 21092747

17. Weinfeld M, Mani RS, Abdou I, Aceytuno RD, Glover JN (2011) Tidying up loose ends: the role of polynucleotide kinase/phosphatase in DNA strand break repair, Trends Biochem Sci, 36, 262–71. doi: 10.1016/j.tibs.2011.01.006 PMID: 21353781

18. Mandal SM, Hegde ML, Chatterjee A, Hedge PM, Szczesny B et al, (2012) Role of human DNA glycosylase Nei-like 2 (NEIL2) and single strand break repair protein polynucleotide kinase 3'-phosphatase in maintenance of mitochondrial genome, J Biol Chem, 287, 2819–2829. doi: 10.1074/jbc.M111.272179 PMID: 22130663

19. Shyu YJ, Liu H, Deng X, Hu CD (2006) Identification of new fluorescent protein fragments for bimolecular fluorescence complementation analysis under physiological conditions, Biotechniques, 40, 61–66. doi: 10.2144/000112036 PMID: 16454041

20. Weibrecht I, Leuchowius KJ, Clausson CM, Conze T, Jarvius M et al, (2010) Proximity ligation assay: a recent addition to the proteomics toolbox, Expert Rev Proteomics, 7, 401–409. doi: 10.1586/epr.10.10 PMID: 20536310

21. Silva-Fernandes A, Duarte-Silva S, Neves-Carvalho A, Amorim M, Soares-Cunha C et al, (2014) Chronic treatment with 17-DMAG improves balance and co-ordination in a new mouse model of Machado-Joseph disease, Neurotherapeutics, 11, 433–49. doi: 10.1007/s13311-013-0255-9 PMID: 24477711

22. Pacheco LS, da Silveira AF, Trott A, Houenou LJ, Algarve TD et al, (2013) Association between Machado-Joseph disease and oxidative stress biomarkers, Mutat research, 757, 99–103. doi: 10.1016/j.mrgentox.2013.06.023

23. Kurz EU, Lees-Miller SP (2004) DNA damage-induced activation of ATM and ATM-dependent signaling pathways, DNA Repair, 3, 889–900. doi: 10.1016/j.dnarep.2004.03.029 PMID: 15279774

24. Guo Z, Kozlov S, Lavin MF, Person MD, Paull TT (2010): ATM activation by oxidative stress, Science, 330, 517–521. doi: 10.1126/science.1192912 PMID: 20966255

25. Miller FD, Pozniak CD, Walsh GS (2000) Neuronal life and death: an essential role for the p53 family, Cell Death Differ, 7, 880–888. doi: 10.1038/sj.cdd.4400736 PMID: 11279533

26. Culmsee C, Mattson MP (2005) p53 in neuronal apoptosis, Biochem Biophys Res Commun, 331, 761–777. doi: 10.1016/j.bbrc.2005.03.149 PMID: 15865932

27. Chang JR, Ghafouri M, Mukerjee R, Bagashev A, Chabrashvili T et al, (2011) Role of p53 in neurodegenerative diseases, Neurodegener Dis, 9, 68–80. doi: 10.1159/000329999 PMID: 22042001

28. Bae BJ, Xu H, Igarashi S, Fujomoto M, Agrawal N et al, (2005) p53 mediates cellular dysfunction and behavioral abnormalities in Huntington disease, Neuron, 47, 29–41. doi: 10.1016/j.neuron.2005.06.005 PMID: 15996546

29. Wang HL, Chou AH, Lin AC, Chen SY, Weng YH et al, (2010) Polyglutamine-expanded ataxin-7 upregulates Bax expression by activating p53 in cerebellar and inferior olivery neurons. Exp Neurol, 224, 486–494. doi: 10.1016/j.expneurol.2010.05.011 PMID: 20546728

30. Kharbanda S, Pandey P, Jin S, Inoue S, Bharti A et al, (1997) Functional interaction between DNA-PK and c-Abl in response to DNA damage, Nature, 386, 732–735. doi: 10.1038/386732a0 PMID: 9109492

31. Baskaran R, Wood LD, Whitaker LL, Canman CE, Morgan SE et al, (1997) Ataxia telangiectasia mutant protein activates c-Abl tyrosine kinase in response to ionizing radiation, Nature, 387, 516–519. doi: 10.1038/387516a0 PMID: 9168116

32. Shafman T, Khanna KK, Kedar P, Spring K, Kozlov S et al, (1997) Interaction between ATM protein and c-Abl in response to DNA damage, Nature, 387, 520–523. doi: 10.1038/387520a0 PMID: 9168117

33. Yuan ZM, Utsugisawa T, Ishiko T, Nakada S, Huang Y et al, (1998) Activation of protein kinase c-δ by the c-Abl tyrosine kinase in response to ionizing radiation, Oncogene, 16, 1643–1648. doi: 10.1038/sj.onc.1201698 PMID: 9582011

34. Adwan TS, Ohm AM, Jones DNM, Humphries MJ, Reyland ME (2011) Regulated binding of Importin-α to protein kinase-Cδ in response to apoptotic signaling facilitates nuclear import, J Biol Chem, 286, 35716–35724. doi: 10.1074/jbc.M111.255950 PMID: 21865164

35. Basu A, Woolard MD, Johnson CL, (2001) Involvement of protein kinase C-δ in DNA damage-induced apoptosis, Cell Death Differ, 8, 899–908. doi: 10.1038/sj.cdd.4400885 PMID: 11526445

36. Yoshida K (2008): Nuclear trafficking of pro-apoptotic kinases in response to DNA damage, Trends Mol Med, 14, 305–313. doi: 10.1016/j.molmed.2008.05.003 PMID: 18539531

37. Fishel ML, Vasko MR, Kelly MR (2007) DNA repair in the neurons: so if they don't divide what's to repair, Mutat Res, 614, 24–36. doi: 10.1016/j.mrfmmm.2006.06.007 PMID: 16879837

38. Weissman L, de souza-Pinto NC, Stevnsner T, Bohr VA (2007) DNA repair, mitochondria, and neurodegeneration, Neuroscience, 145, 1318–1329. doi: 10.1016/j.neuroscience.2006.08.061 PMID: 17092652

39. LeDoux SP, Druzhyna NM, Hollensworth SB, Harrison JF, Wilson GL (2007) Mitochondrial DNA repair: a critical player in the response of cells of the CNS to genotoxic insults, Neuroscience, 145, 1249–1259. doi: 10.1016/j.neuroscience.2006.10.002 PMID: 17097236

40. Halliwell B (2006) Oxidative stress and neurodegeneration: where are we now? J Neurochem, 97, 1634–1658. doi: 10.1111/j.1471-4159.2006.03907.x PMID: 16805774

41. Ryter SW, Kim HP, Hoetzel A, Park JW, Nakahira K et al, (2007) Mechanism of cell death in oxidative stress, Antioxid Redox Signal, 9, 49–89. doi: 10.1089/ars.2007.9.49 PMID: 17115887

42. Wilson DM and McNeil DR 3rd, (2007) Base excision repair and the central nervous system, Neuroscience, 145, 1187–1200. doi: 10.1016/j.neuroscience.2006.07.011 PMID: 16934943

43. Lee Y, McKinnon PJ (2007) Responding to DNA double strand breaks in the nervous system, Neuroscience, 145, 1365–1374. doi: 10.1016/j.neuroscience.2006.07.026 PMID: 16934412

44. Date H, Onodera O, Tanaka H, Iwabuchi K, Uekawa K et al, (2001) Early-onset ataxia with ocular motor apraxia and hypoalbuminemia is caused by mutation in a new HIT superfamily gene, Nat Genet, 29, 184–8. doi: 10.1038/ng1001-184 PMID: 11586299

45. Moreira MC, Barbot C, Tachi N, Kozuka N, Uchida E, et al, (2001) The gene mutated in ataxia-ocular apraxia 1 encodes the new HIT/Zn-finger protein aprataxin, Nat Genet, 29, 189–93. doi: 10.1038/ng1001-189 PMID: 11586300

46. Takashima H, Boerkoel CF, John J, Saifi GM, Salih MA et al, (2002) Mutation of TDP1, encoding a topoisomerase I-dependent DNA damage repair enzyme, in spinocerebellar ataxia with axonal neuropathy, Nat Genet, 32, 267–72. doi: 10.1038/ng987 PMID: 12244316

47. Wang W-Y, Pan L, Su SC, Quinn EJ, Sasaki M et al, (2013) Interaction of FUS and HDAC1 regulates DNA damage response and repair in neurons, Nat Neurosci, 16, 1383–1391. doi: 10.1038/nn.3514 PMID: 24036913

48. Shen J, Gilmore EC, Marshall CA, Haddadin M, Reynolds JJ et al, (2010) Mutation in PNKP cause microcepgaly, seizures and defects in DNA repair, Nat Genet, 42, 245–9. doi: 10.1038/ng.526 PMID: 20118933

49. Poulton C, Oegema R, Heijsman D, Hoogeboom J, Schot R et al, (2013) Progressive cerebellar atrophy and polyneuropathy: expanding the spectrum of PNKP mutations, Neurogenetics, 14, 43–51. doi: 10.1007/s10048-012-0351-8 PMID: 23224214

50. Reynolds JJ, Walker AK, Gilmore EC, Walsh CA, Caldecott KW (2012) Impact of PNKP mutations associated with microcephaly, seizures and developmental delay on enzyme activity and DNA strand break repair, Nucleic Acids Res, 40, 6608–19. doi: 10.1093/nar/gks318 PMID: 22508754

51. Liu W, Jiang F, Bi X, Zhang YQ (2012) Drosophila FMRP participates in the DNA damage response by regulating G2/M cell cycle checkpoint and apoptosis, Hum Mol Genet, 21, 4655–4668. doi: 10.1093/hmg/dds307 PMID: 22843500

52. Alpatov R, Lesch BJ, Nakamoto-Kinoshita M, Blanco A, Chen S, Stutzer A et al, (2014) A chromatin-dependent role of the Fragile X mental retardation protein FMRP in the DNA damage response, Cell, 157, 869–881. doi: 10.1016/j.cell.2014.03.040 PMID: 24813610

53. Zhang W, Cheng Y, Li Y, Chen Z, Jin P, Chen D (2014) A feed-forward mechanism involving Drosophila fragile X mental retardation protein triggers a replication stress-induced DNA damage response, Hum Mol Genet, 23, 5188–5196. doi: 10.1093/hmg/ddu241 PMID: 24833720

54. Polidori MC, Mecocci P, Browne SE, Senin U, Beal MF (1999) Oxidative damage to mitochondrial DNA in Huntington disease, Neurosci Lett, 272, 53–6. doi: 10.1016/S0304-3940(99)00578-9 PMID: 10507541

55. Rolig RL and McKinnon PJ (2000) Linking DNA damage and neurodegeneration, Trends Neurosci, 23, 417–24. doi: 10.1016/S0166-2236(00)01625-8 PMID: 10941191

56. Martin LJ (2008) DNA damage and repair: Relevance to mechanism of neurodegeneration, J of Neuropathol Exp Neurol, 67, 377–387. doi: 10.1097/NEN.0b013e31816ff780

57. Coppede F, Migliore L (2009) DNA damage and repair in Alzheimer disease, Curr Alzheimer Res, 6, 36–47. doi: 10.2174/156720509787313970 PMID: 19199873

58. Muller SK, Bender A, Laub C, Hogen T, Schlaudraff F et al, (2013) Lewy body pathology is associated with mitochondrial DNA damage in Parkinson disease, Neurobiol Aging, 34, 2231–3. doi: 10.1016/j.neurobiolaging.2013.03.016 PMID: 23566333

59. Yoshida K, Miki Y (2010) The cell death machinery governed by the p53 tumor suppressor in response to DNA damage, Cancer Science, 101, 831–5. doi: 10.1111/j.1349-7006.2009.01488.x PMID: 20132225

60. Oda E, Ohki R, Murasawa H, Nemoto J, Shibue T et al, (2000) Noxa, a BH3-only member of the Bcl-2 family and candidate mediator of p53-induced apoptosis, Science, 288, 1053–8. doi: 10.1126/science.288.5468.1053 PMID: 10807576

61. Fridman JS, Lowe SW (2003) Control of apoptosis by p53, Oncogene, 22, 9030–9040. doi: 10.1038/sj.onc.1207116 PMID: 14663481

62. Chipuk JE, Kuwana T, Bouchier-Hayes L, Droin NM, Newmeyer DD et al, (2004) Direct activation of BAX by p53 mediates mitochondrial membrane permeabilization and apoptosis, Science, 303, 1010–1014. doi: 10.1126/science.1092734 PMID: 14963330

63. Shibue T, Takeda K, Oda E, Tanaka H, Murasawa H et al, (2003) Integral role of Noxa in p53-mediated apoptotic response, Genes Dev, 17, 2233–2238. doi: 10.1101/gad.1103603 PMID: 12952892

64. Nakano K and Vousden KH (2001) PUMA, a novel proapoptotic gene, is induced by p53, Mol Cell, 7, 683–694. doi: 10.1016/S1097-2765(01)00214-3 PMID: 11463392

65. Du C, Fang M, Li L, Wang X (2000) Smac, a mitochondrial protein that promotes cytochrome c-dependent caspase activation by eliminating IAP inhibition, Cell, 102, 33–42. doi: 10.1016/S0092-8674(00)00008-8 PMID: 10929711

66. Cregan SP, Arbour NA, Maclaurin JG, Callaghan SM, Fortin A et al, (2004) p53 activation domain 1 is essential for PUMA upregulation and p53-mediated neuronal cell death, J Neurosci, 24, 10003–10012. doi: 10.1523/JNEUROSCI.2114-04.2004 PMID: 15525786

67. Chipuk JE, Green DR (2006) Dissecting p53-dependent apoptosis, Cell Death Differ, 13, 94–1002. doi: 10.1038/sj.cdd.4401908

68. Bharti A, Kraeft SK, Gounder M, Pandey P, Jin S et al, (1998) Inactivation of DNA-dependent protein kinase by protein kinase C-δ: implication for apoptosis, Mol Cell Biol, 18, 6719–6728. PMID: 9774685

69. Castel AL, Cleary JD, Pearson CE (2010) Repeat instability as the basis for human diseases and as a potential target for therapy, Nat Rev, 11, 165–170. doi: 10.1038/nrm2854

70. Mason AG, Tome S, Simard JP, Libby RT Bammler TK, Beyer RP et al (2014) Expression levels of DNA replication and repair genes predict regional somatic repeat instability in the brain but not altered by polyglutamine disease protein expression or age, Hum Mol Genet, 23, 1606–1618. doi: 10.1093/hmg/ddt551 PMID: 24191263

Cerebral Cortex, 2015, 1–13

doi: 10.1093/cercor/bhu308
Original Article

ORIGINAL ARTICLE

Two Types of Neurons in the Primate Globus Pallidus External Segment Play Distinct Roles in Antisaccade Generation

Atsushi Yoshida[1,2] and Masaki Tanaka[1]

[1]Department of Physiology, and [2]Department of Diagnostic and Interventional Radiology, Hokkaido University School of Medicine, Sapporo 060-8638, Japan

Address correspondence to Dr Atsushi Yoshida, Departments of Physiology and Diagnostic and Interventional Radiology, Hokkaido University School of Medicine, North 15, West 7, Sapporo 060-8638, Japan. Email: yoshidaatsushi0113@gmail.com or Dr Masaki Tanaka, Department of Physiology, Hokkaido University School of Medicine, North 15, West 7, Sapporo 060-8638, Japan. Email: masaki@med.hokudai.ac.jp

Abstract

The globus pallidus external segment (GPe) constitutes part of the indirect pathway of the basal ganglia. Because of inhibitory projections from the striatum, most GPe neurons are expected to reduce activity during movements. However, many GPe neurons in fact display increased activity. We previously found that both excitatory and inhibitory responses were modulated during antisaccades, when eyes were directed away from a visual stimulus. To elucidate the roles of these neurons during antisaccades, we examined neuronal activities as monkeys performed antisaccades, prosaccades, and NoGo tasks under 2 conditions. In the Deliberate condition, the task-rule was instructed by color of the fixation point, while in the Immediate condition, it was given by color of the target. Under both conditions, the increase-type neurons exhibited greater activity during antisaccades compared with the other tasks and neuronal activity negatively correlated with saccade latency. The decrease-type neurons also showed greater modulation during antisaccades but their activity was comparable between NoGo and antisaccade trials in the Immediate condition. These results suggest that the increase-type neurons might play a role in facilitating antisaccades, whereas the decrease-type neurons could mediate signals for reflexive saccade suppression. We propose that these GPe neurons are differently involved in basal ganglia pathways.

Key words: antisaccade, globus pallidus external segment, physiology, primate

Introduction

A widely accepted view regarding the neuronal processes in the basal ganglia assumes the "direct" and "indirect" pathways (Albin et al. 1989; DeLong 1990). Although this hypothesis can explain many pathophysiological aspects of basal ganglia diseases, including Parkinson's disease, the growing body of evidence suggests that this hypothesis might be too simplistic; in addition to the alternative direct and indirect pathways, several other major projections in the basal ganglia have recently been elucidated (for reviews, see Nambu et al. 2002; Wichmann et al. 2011). According to the original hypothesis, the external segment of the globus pallidus (GPe) constitutes part of the indirect pathway, which plays a role in the suppression of actions (Brotchie et al. 1991; for review, see Chan et al. 2005). Because of the inhibitory projection from the striatum, neurons in the GPe are expected to exhibit decreased activity during movements. However, more than half of the neurons in the GPe in fact exhibit increased activity during movements (Mitchell et al. 1987; Turner and Anderson 1997; Yoshida and Tanaka 2009a,b; Shin and Sommer 2010; for review, see Goldberg and Bergman 2011), suggesting that the direct excitatory inputs from the subthalamic nucleus (STN) might regulate neuronal activity in the GPe (Shink et al. 1996) (Fig. 1D).

Although the firing properties of 2 types of neurons in the GPe have been well documented, their functional roles remain

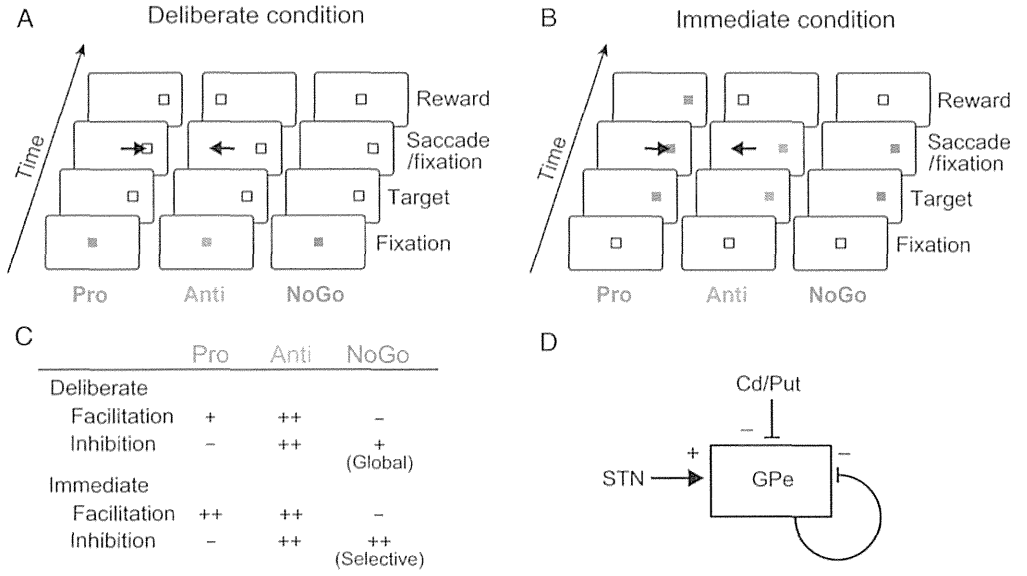

Figure 1. Behavioral paradigms and underlying neuronal processes. (*A*) Sequence of events in the Deliberate condition, in which color of the fixation point indicates the task-rule. A target spot appeared 12° right or left at the time of the fixation point offset. Monkeys were required to make a saccade away from (antisaccade) or toward (prosaccade) the target within 400 ms, or maintain fixation for >400 ms (NoGo). (*B*) In the Immediate condition, task-rule was indicated by color of the saccade target. This imposed monkeys to select an action immediately, as they were not informed of the trial type in advance. Different trials were randomly interleaved in a block. Anti, antisaccade; Pro, prosaccade. (*C*) In each task and condition, the brain needs to facilitate or inhibit saccade production. Note that the inhibitory processes during the NoGo trials differ between the conditions. (*D*) Anatomical connections of the GPe. Neurons in the GPe receive both excitatory (glutamatergic) and inhibitory (GABAergic) projections. Cd, caudate nucleus; GPe, external segment of the globus pallidus; Put, putamen.

elusive. Previously we examined GPe neurons responding to saccades, and found that both types of neurons exhibited enhanced firing modulation during antisaccades, when eyes were directed away from the target (Yoshida and Tanaka 2009a). These neurons could have a role in the production of antisaccade commands and/or the suppression of reflexive saccades toward the target, both of which are indispensable neural processes for the generation of antisaccades (Munoz and Everling 2004). Indeed, our previous study showed that inactivation of the GPe with muscimol resulted in the increased number of erroneous antisaccades (Yoshida and Tanaka 2009a).

The purpose of the present study was to elucidate the roles of signals in the GPe in the generation of antisaccades. In addition to the antisaccade and prosaccade trials, we randomly introduced the NoGo trial so as to dissociate the saccade-related movement activity from that related to saccade suppression. Recent studies suggest that there are 2 types of proactive inhibitory controls during antisaccades (Abegg et al. 2012). The "global suppression" withholds any motor response, causing general lengthening of reaction time, whereas the "selective suppression" inhibits a particular response that could be directed to distractive stimuli. These 2 processes appear to be regulated by different pathways in the basal ganglia (Majid et al. 2013; for review, see Aron 2011).

To examine these inhibitory processes, we presented trials in 2 different conditions. In one condition, the task-rule was given by the color of the fixation point in advance of the target appearance (Deliberate condition, Fig. 1A). In this condition, the global suppression may dominate during the NoGo trials in which the subjects should ignore visual stimuli and maintain fixation throughout the trial (Fig. 1A). In the other condition, the task-rule was indicated by the color of the target (Immediate condition, Fig. 1B). Because the subjects need to direct attention to the visual stimuli rather than simply ignoring them even in the NoGo trials, the signals related to selective suppression should be generated in the absence of movements. Thus, using the 3 tasks in 2 different conditions, we were able to examine neuronal activity related to saccade production or suppression, and to dissociate signals related to global suppression from selective suppression (Fig. 1C). Our data show that the increase-type neurons exhibited different firing properties from the decrease-type neurons during the trials, suggesting that the 2 types of GPe neurons might be differently involved in antisaccade generation, one facilitating and the other suppressing saccades.

Materials and Methods

Animal Preparation

Experiments were conducted on 4 Japanese macaques (*Macaca fuscata*, one 7 kg male and three 4–6 kg females). All experimental protocols were approved by the Animal Care and Use Committee of Hokkaido University. The experimental procedures were similar to those described previously (Tanaka 2005). After initial chair training, a pair of head holders was implanted in the skull using titanium screws and dental acrylic under general isoflurane anesthesia and using sterile procedures. To induce anesthesia, we administered medetomidine (40 μg/kg) and midazolam (0.3 mg/kg) intramuscularly. The animals were intubated to maintain anesthesia using a mixture of isoflurane (1–3%), nitrous oxide, and oxygen. In a separate surgical procedure, a coil of stainless steel wire was implanted under the conjunctiva to record eye movements. During subsequent training and experimental sessions, the monkey's head was fixed to the primate chair, and horizontal and vertical eye position was recorded using the search coil technique. After sufficient training for eye movement tasks, a recording cylinder was installed over a small craniotomy under the same surgical conditions as above.

Animals received analgesics (pentazocine or ketoprofen) during each surgery and for several days subsequently. Topical antibiotics were administered around the implant and in the cylinder as necessary. Water intake was controlled daily so that monkeys were motivated to perform behavioral tasks.

Visual Stimulus and Behavioral Paradigms

Experiments were controlled by a Windows-based real-time data acquisition system (TEMPO; Reflective Computing, St. Louis). All events were updated every 5 ms, and visual stimuli were presented on a 24-inch cathode-ray tube monitor (GDM-FW900; Sony, Tokyo; refresh rate: 60 Hz) that was located 38 cm away from the eyes, and subtended visual angle of 64 × 44°. A 0.5° square spot served as a visual stimulus. Targets of different colors (white, red, green, and blue) were used for different means in each trial (see below). Experiments were carried out in a darkened booth. Voltages proportional to horizontal and vertical eye position were calibrated before each experiment by having monkeys fixate on a stationary target spot at known visual angles. Thereafter, visual stimuli were presented in individual trials, and monkeys were rewarded at specific time intervals during each trial with drops of water or apple juice for maintaining eye position within a "window" that surrounded the stimulus position. The size of the window was 2° for initial fixation, 6° (antisaccade task) or 3° (prosaccade task) for the saccade target, and 5° for the maintenance of fixation during target presentation in the NoGo trials. A trial was aborted and followed by a newly selected trial if monkeys failed to maintain eye position within a specified window. Trials of different types and in different directions were presented in a random order within a block. The saccade target was presented either 12° left or right of the fixation point.

The present study used 3 tasks in 2 conditions (Fig. 1). In the Deliberate condition, the task-rule was given by color of the fixation point in advance of the target appearance. In contrast, in the Immediate condition, the task-rule was given by color of the peripheral target so that monkeys were unable to prepare for specific action until the target was presented. We used 4 colors (white, red, green, and blue) for the fixation point and the target. Contrast modulation (Michelson contrast) was calculated for each stimulus using the formula $C_M = (A - B)/(A + B)$, where A was the luminance of a given stimulus and B was the luminance of the background on the screen (1.59 cd/m^2). In all tasks, the fixation point initially appeared at the center of the screen for 1600 ms. In trials with either a green fixation point ($C_M = 9.18$, Deliberate condition) or a green saccade target (Immediate condition), monkeys were required to perform antisaccades 180° away from the target within 400 ms. In trials with a red fixation point or saccade target ($C_M = 5.10$), monkeys were required to perform prosaccades. When either a blue fixation point or a blue saccade target ($C_M = 3.77$) was presented, the animals were required to maintain central fixation for >400 ms following the target onset. The saccade target in the Deliberate condition and the fixation point in the Immediate condition were always white ($C_M = 14.21$, Fig. 1A,B). In both saccade tasks, the peripheral target disappeared after a second fixation interval of 500 ms, and then a liquid reward was given. Introduction of the second fixation interval allowed us to temporally dissociate the neuronal responses to eye movements from those to reward.

Recording Procedures

Tungsten microelectrodes (FHC, Bowdoin, ME) were lowered through a 23-gauge stainless steel tube guided by a grid system (Crist Instrument Co.). The electrodes were advanced using a hydraulic micromanipulator (MO-97S; Narishige, Tokyo) attached to the recording cylinder, which allowed vertical (monkey S) or 38–40° off-vertical penetrations (monkeys U, V, and X) in the coronal plane. Signals obtained from the electrodes were amplified, filtered, and monitored using oscilloscopes and an audio monitor. Once task-related neuronal activity was encountered, spikes of single neurons were isolated using a real-time spike sorter with template-matching algorithms (MSD; Alpha Omega Engineering, Nazareth, Israel). For each experiment, the occurrence of action potentials was time-stamped and saved in files with the data of eye movements, location and timing of visual stimuli.

Data Acquisition and Analysis

Horizontal and vertical eye position signals were directly obtained from the eye coil electronics (MEL-25; Enzanshi Kogyo, Chiba, Japan). Data were digitized and sampled at 1 kHz, and were stored in files during the experiments for further off-line analysis, performed using Matlab (Mathworks, Natick, MA). For each neuron, data were aligned with either the initiation of saccades or the target onset. In some antisaccade trials, monkeys initially generated a saccade toward the target, but redirected their eyes to the location opposite to the target within 400 ms ("turn-around saccade"). Since we detected error trials by analyzing eye position before and 400 ms after the fixation point offset during experiments, monkeys were rewarded in such trials. We detected turn-around saccades off-line and considered them as errors and these data were excluded from the subsequent analyses. Traces of horizontal and vertical eye positions were reviewed with rasters and spike density profiles that were constructed from neuronal data.

Neurons recorded during fewer than 10 trials for each task condition were excluded from subsequent analyses. Neuronal activity was measured during the following 3 time periods: (1) the 300-ms interval immediately before the fixation point onset (baseline period); (2) the 250-ms period after the target onset (target onset period); and (3) the 150-ms period starting from 100 ms before saccades (saccade period). We used a relatively long target onset period to compare neuronal activities during antisaccades with those during NoGo trials, because reaction times of antisaccades were ~250 ms and the suppression of reflexive saccades should have occurred during this interval in the NoGo trials. We defined neuronal activity as "antisaccade-related" when it differed significantly from the baseline activity during antisaccades (2-tailed paired t test, $P < 0.05$). These neurons were further classified into 2 groups, "increase-type" or "decrease-type", according to the direction of firing modulation during antisaccades. The time course of neuronal activity for each condition was examined qualitatively by calculating the spike density function using a Gaussian filter ($\sigma = 15$ ms). However, all quantitative measures were performed on the basis of spike counts for specific time windows. Analytical measures are reported in the relevant text in the Results. To evaluate neuronal activity, the mean firing rate was assessed using the analysis of variance (ANOVA) followed by post hoc multiple comparisons (Scheffé's method). Each statistical test that was applied is stated in the relevant text in the Results.

Verification of the Recording Sites

The recording sites were reconstructed based on magnetic resonance images [MRI; GE Signa 1.5 T; 3D T_1-weighted images (1 mm

thick slice) and 2D T_2-weighted images (1.5 mm thick slice)] after implantations of the recoding chamber. Consistent with our previous study (Yoshida and Tanaka 2009a), many antisaccade-related neurons were found in the anterior part of the GPe, close to the anterior commissure (Fig. 2).

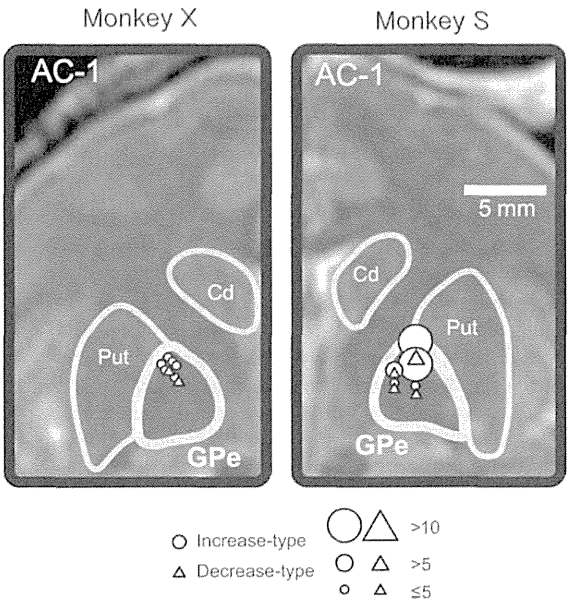

Figure 2. Sites of the task-related neurons are overlaid on MR images shown in the frontal sections (T_2-weighted image). Left panel shows the left hemisphere of monkey X, while right panel shows the right hemisphere of monkey S. Shape of symbols indicates response property, and the size indicates the number of recorded neurons. Both MR images are the sections 1 mm posterior to the anterior commissure (AC). Cd, caudate nucleus; GPe, external segment of the globus pallidus; Put, putamen; STN, subthalamic nucleus.

Results

Database and Recording Sites

Data were collected only after monkeys were well trained on the 3 tasks under both conditions. Table 1 summarizes the behavioral data obtained during 170 recording sessions. All monkeys performed the task correctly in >88% of trials. Error trials in the antisaccade task contained those with reflexive saccades toward the visual stimuli (including turn-around saccades) and those without saccades during 400 ms of target appearance. Overall, a 2-way ANOVA revealed that saccade latencies were statistically different between conditions (192 ± 48 ms and 241 ± 50 ms for the Deliberate and Immediate conditions, respectively, $P < 0.05$) as well as between pro- (204 ± 56 ms) and antisaccades (230 ± 51 ms, $P < 0.05$). There was also a significant interaction between the main factors ($P < 0.05$), indicating that the difference in latency between the 2 saccade tasks was statistically greater in the Deliberate condition than in the Immediate condition.

We recorded from 170 single GPe neurons in 6 hemispheres of 4 monkeys ($n = 102$, 34, 20, and 14 for monkeys S, X, U, and V, respectively) that modulated their activity in association with saccades. More than 2 thirds of these neurons increased their firing rates before and during saccades ("increase-type" neurons, $n = 117$, 70%), whereas the remaining neurons decreased their firing rate ("decrease-type" neurons, $n = 53$, 30%). For the 4 animals, the proportion of the increase-type neurons ranged from 62–80% (increase/decrease, 70/32, 21/13, 16/4, 10/4, for monkeys S, X, U, and V, respectively).

Figure 2 illustrates the recording sites overlaid on MR images of monkeys X and S. Most saccade-related neurons were found in the anterodorsal part of the GPe, within 2 mm anterior or posterior to the level of the anterior commissure, consistent with our previous study (Yoshida and Tanaka 2009a). Anatomical studies have shown that this part of the GPe receives projections from the associative areas in the striatum (Haber et al. 1993; Francois et al. 1994, 2004; for review, see Parent and Hazrati 1995b). Our

Table 1 Comparison of behavioral parameters between conditions

	Deliberate			Immediate		
	Anti	Pro	NoGo	Anti	Pro	NoGo
Monkey S						
N (correct/all)	4539/4573	4548/4549	4570/4751	4549/4574	4569/4581	4581/4617
Error rate (%)	0.7	0.0	3.8	0.5	0.3	0.8
Latency (ms)	215 ± 30	188 ± 31	—	254 ± 30	247 ± 30	—
Error latency	139 ± 51	—	—	157 ± 17	224 ± 21	—
Monkey X						
N (correct/all)	1293/1296	1289/1292	1288/1425	1288/1289	1293/1293	1293/1326
Error rate (%)	0.0	0.0	10.6	0.0	0.0	2.50
Latency (ms)	300 ± 39	262 ± 22	—	325 ± 30	324 ± 32	—
Error latency	213 ± 36	—	—	—	—	—
Monkey V						
N (correct/all)	749/851	848/848	852/853	824/854	851/851	842/842
Error rate (%)	11.7	0.0	0.0	3.5%	0.0	0.0
Latency (ms)	223 ± 52	182 ± 48	—	295 ± 40	193 ± 59	—
Error latency	149 ± 14	—	—	206 ± 37	—	—
Monkey U						
N (correct/all)	426/428	425/425	435/440	423/425	427/427	428/434
Error rate (%)	0.5	0.0	1.1	0.5	0.0	1.4
Latency (ms)	224 ± 32	185 ± 26	—	274 ± 31	260 ± 37	—
Error latency	199 ± 44	—	—	223 ± 29	—	—

Values of latency indicate mean ± SD.

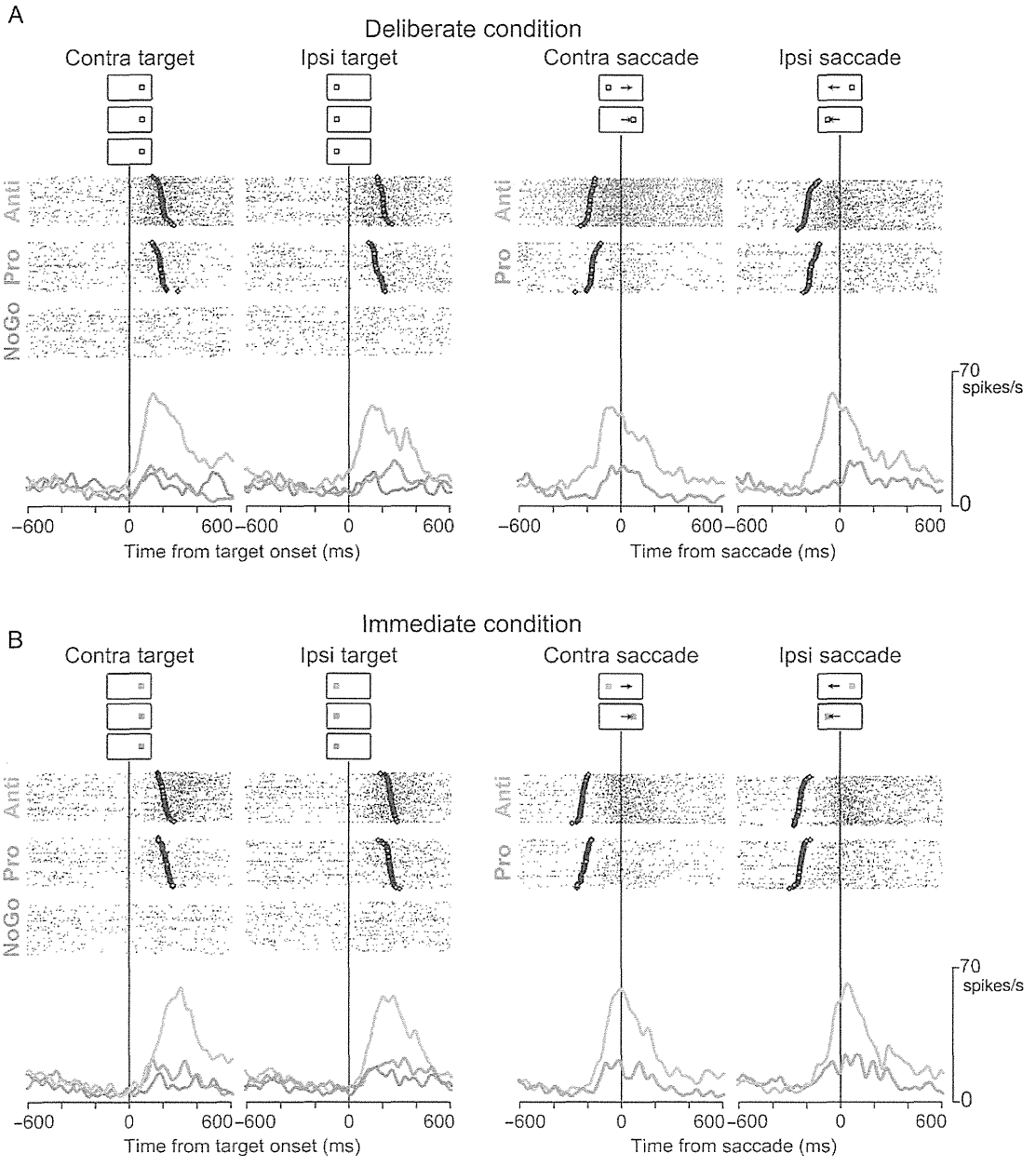

Figure 3. Comparison of the responses between paradigms for representative increase-type neuron. (A) Deliberate condition. (B) Immediate condition. In all panels, data are aligned on the target onset or saccade initiation (vertical lines). Raster lines are sorted according to saccade latency. Traces in different colors indicate spike density for different conditions. The diamond on each raster line indicates the time of saccade initiation (left two panels) or target onset (right 2 panels). Anti, antisaccade; Pro, prosaccade.

recording sites appeared to be somewhat anterior to the sites in other studies that had been examined for saccade-related neuronal activity (Kato and Hikosaka 1995; Shin and Sommer 2010).

Properties of Increase-type Neurons

Figure 3 plots the data of a representative increase-type neuron under 2 different conditions. As the data were aligned to the initiation of saccades, neuronal activity just before antisaccades was greater than that before prosaccades under the Deliberate condition (Fig. 3A, right 2 panels), which is consistent with our previous study (Yoshida and Tanaka 2009a). This neuron also exhibited an enhanced activity during antisaccades under the Immediate condition (Fig. 3B, right 2 panels), while the gradual elevation of firing rate at the time of target onset found in the Deliberate condition disappeared (left panels). To examine whether the GPe was involved in the suppression of reflexive saccades, we randomly introduced the NoGo trials under both conditions. Neuronal activity in the NoGo trials under the Deliberate condition was expected to be related to global saccade suppression, while that under the Immediate condition was likely to be related to selective suppression (Abegg et al. 2012; Fig. 1C). When the data were aligned to the target onset, neuronal activity in the NoGo trials was less than that during antisaccades under

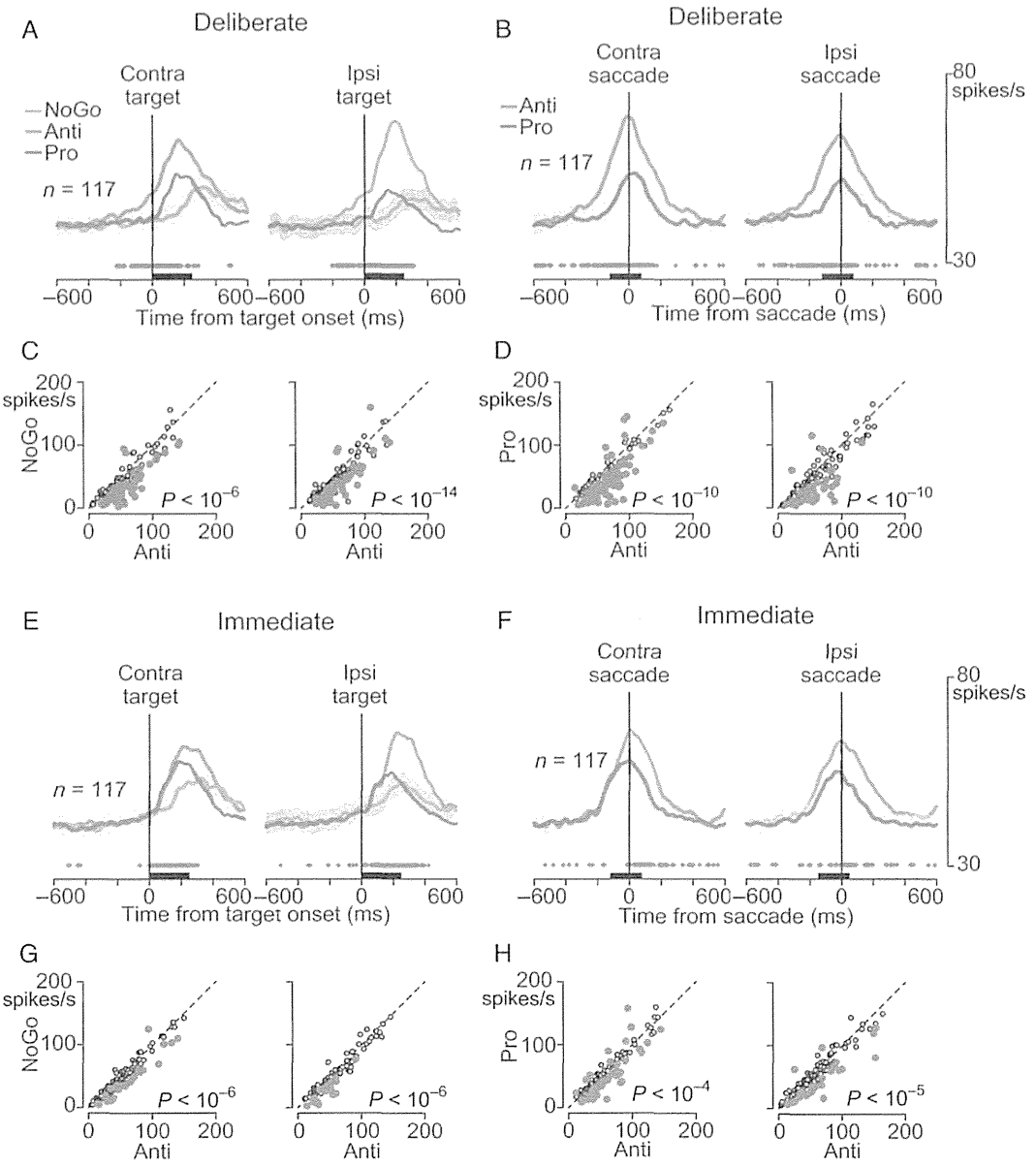

Figure 4. Quantitative analyses of the increase-type neurons. (*A*) and (*B*) Time courses of the population activity following the target onset (*A*) or saccade initiation (*B*) under the Deliberate condition. The shaded areas indicate ± SEMs. The magenta raster below the traces indicate 25-ms time intervals when neuronal activity during antisaccades differed from that during NoGo trials (*A*) or prosaccades (*B*). (*C*) and (*D*) Comparison of the firing rate of individual neurons during antisaccades with that during NoGo trials (*C*) or prosaccades (*D*) under the Deliberate condition. Neuronal activity was measured for a 250-ms interval following the target onset (black bars in *A*) or a 150-ms interval starting from 100 ms before saccade initiation (black bars in *B*). Red symbols indicate the data with a significant difference ($P < 0.05$). (*E*) and (*F*) Time courses of the population activity under the Immediate condition. Conventions are the same as in (*A*) and (*B*). (*G*) and (*H*) Each data point compares the firing rate of individual neurons during antisaccades with that during the other tasks under the Immediate condition.

both conditions (Fig. 3A,B, left 2 panels), suggesting that this neuron might not be involved in any type of saccade suppression.

To examine the time course of neuronal activity, Figure 4 plots the population activities of the increase-type neurons during different conditions. The traces in Figure 4A,E show that neuronal activities during the NoGo trials were consistently less than those during antisaccades. For individual neurons, Figure 4C,G compare the mean firing rate during 250 ms following the target onset between the antisaccade and NoGo trials. Under the Deliberate condition, 59 (50%) and 55 (47%) out of 117 increase-type neurons displayed activities that were statistically different between the trials for contralateral and ipsilateral targets, respectively (2-way ANOVA, $P < 0.05$, followed by Scheffé's test, $P < 0.05$, Fig. 4C, red symbols). Under the Immediate condition, 26 (22%) and 23 (19%) of neurons showed differential activity between the trials for contralateral and ipsilateral targets, respectively ($P < 0.05$, Fig. 4G). In the whole population, the activity immediately after the target onset in the antisaccade trials was statistically greater than that during the NoGo trials for all combinations of target locations and task conditions (paired t test, $P < 10^{-6}$), suggesting that these neurons might play only a minor role in saccade suppression. Although many neurons exhibited a gradual elevation of activity prior to target onset during antisaccade trials under the Deliberate condition (Fig. 4A), the baseline

activity during stable fixation (500–1000 ms before target onset) did not differ either between conditions or paradigms (2-way ANOVA, $P = 0.66$), indicating that the variation of neuronal activity during initial fixation did not solely reflect the difference in visual attributes.

To estimate the timing of when neuronal activity during antisaccades differed from that during the NoGo trials, we performed time-series analysis for every 25-ms window starting from 600 ms before and ending at 600 ms following the target onset. The rasters below the traces of population activities in Figure 4A,E summarize the statistical results (Mann Whitney *U*-test, $P < 0.05$). When the neuronal differentiation time was defined as the center of the first bin of 10 consecutive intervals with significant difference, the values were −177 ms (contralateral target) and −124 ms (ipsilateral target) for the Deliberate condition, and 27 ms (contra) and 49 ms (ipsi) for the Immediate condition.

The enhancement of neuronal activity during antisaccades suggested a role of the increase-type neurons in the production of volitional saccade commands. To test this, we next examined neuronal activity around the times of saccades. Figure 4B,F show the time courses of the population activity during saccades under the 2 different conditions. The increase-type neurons exhibited enhanced activity during antisaccades compared with that during prosaccades, in particular, under the Deliberate condition (Fig. 4B). To assess the saccade-related activities, the firing rates of individual neurons were measured for a 150-ms interval starting from 100 ms prior to saccades (Fig. 4B,F, black bars). A 2-way ANOVA and the following multiple comparisons revealed that neuronal activity was greater during anti- compared with prosaccades for 30% ($n = 35/117$, contraversive saccades) and 23% ($n = 27$, ipsiversive saccades) of neurons under the Deliberate condition, and for 55% ($n = 64$, contra) and 34% ($n = 40$, ipsi) of neurons under the Immediate condition (Scheffé's test $P < 0.05$; Fig 4D,H, red symbols). In the whole population, the magnitude of neuronal activity during antisaccades was greater than that during prosaccades (paired t test, $P < 10^{-4}$ and $P < 10^{-10}$ for the Deliberate condition and the Immediate condition, respectively). When we measured the neuronal differentiation time between antisaccade and prosaccade tasks, the values were −325 ms (contralateral saccades) and −263 ms (ipsilateral saccades) in the Deliberate condition, and −21 ms (contra) and −103 ms (ipsi) in the Immediate condition.

To further examine whether the increase-type neurons played a role in saccade generation, trials from each neuron were divided into tertiles according to saccade latencies. Traces in the upper panels of Figure 5A,B show the population activities for the 3 groups aligned to the target onset in contraversive antisaccade trials. Although neuronal activity for trials with shorter latencies was greatest during antisaccades in both conditions, the activity was relatively comparable between groups during prosaccades. When rank correlation between the firing rates (−100 to 50 ms of the target onset) and individual saccade latencies was computed for each neuron, the mean of correlation coefficients was statistically smaller than zero (one sample *t* test, $n = 117$, $P < 0.05$) during antisaccades under all 4 combinations of saccade direction and trial condition. In contrast, the mean of rank correlation coefficients did not differ from zero during prosaccades ($P > 0.05$). These results suggest that the increase-type neurons might play a role in facilitating antisaccades.

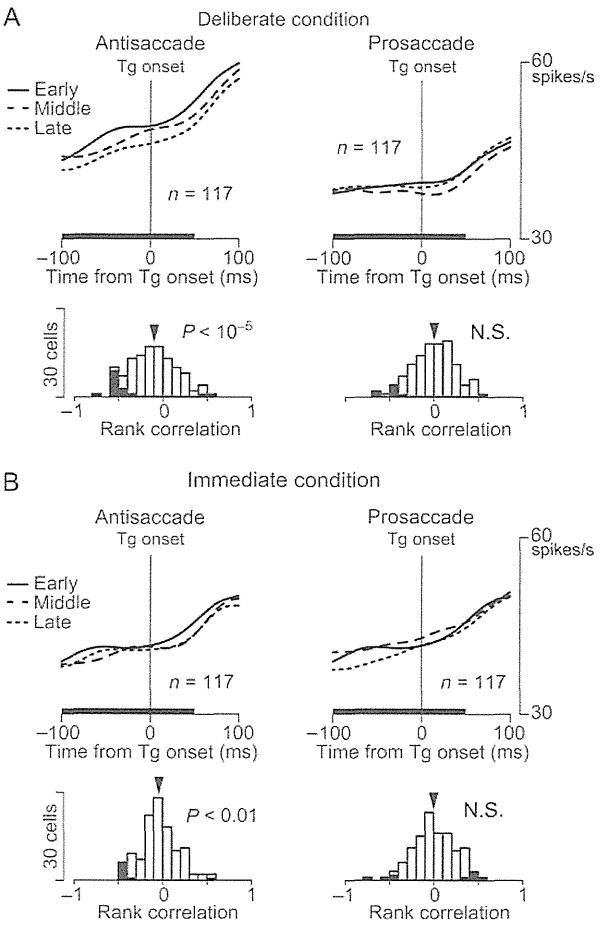

Figure 5. Correlation between neuronal activity and saccade latency. (*A*) Time courses of population activity for contraversive saccades in the Deliberate condition. For each neuron, the data were divided into 3 groups with equal number of trials according to saccade latencies. The population activity was computed for each of the 3 groups shown in different line styles. The lower histograms indicate the distributions of correlation coefficients computed between neuronal activities (−100 to 50 ms of target onset, black bar in the upper panel) and individual saccade latency. Arrowhead above each histogram indicates the mean value which was significantly smaller than zero for antisaccades (one-sided *t* test, $P < 10^{-5}$) but not for prosaccades. (*B*) Data for the Immediate condition. Conventions are the same as in (*A*).

Properties of Decrease-type Neurons

Figure 6 plots the data from a representative decrease-type neuron. This neuron reduced activity in a similar manner during all 3 tasks under the Immediate condition (Fig. 6B), whereas, under the Deliberate condition, the size of the firing modulation was greatest during antisaccades (Fig. 6A). Similarly to previously reported neurons (Yoshida and Tanaka 2009a), this neuron started to modulate activity even during the instruction period when the task-rule was presented, possibly because the monkey prepared for antisaccades even though the target location was still uncertain. For multiple decrease-type neurons ($n = 53$), Figure 7A,E compare the time courses of the population activities between different trials under both conditions. Unlike the increase-type neurons (Fig. 4E), neuronal activity during the NoGo trials was similar to that during antisaccades under the Immediate condition (Fig. 7E). When the firing rates of individual decrease-type neurons were measured for 250 ms from the target onset (black bars in Fig. 7A,E), 15 (28%, contralateral target) and 10 (19%, ipsilateral target) neurons exhibited differential activity between the antisaccade trials and the NoGo trials under the Deliberate condition, and 5 (9%, contra) and 2 (4%, ipsi) neurons exhibited

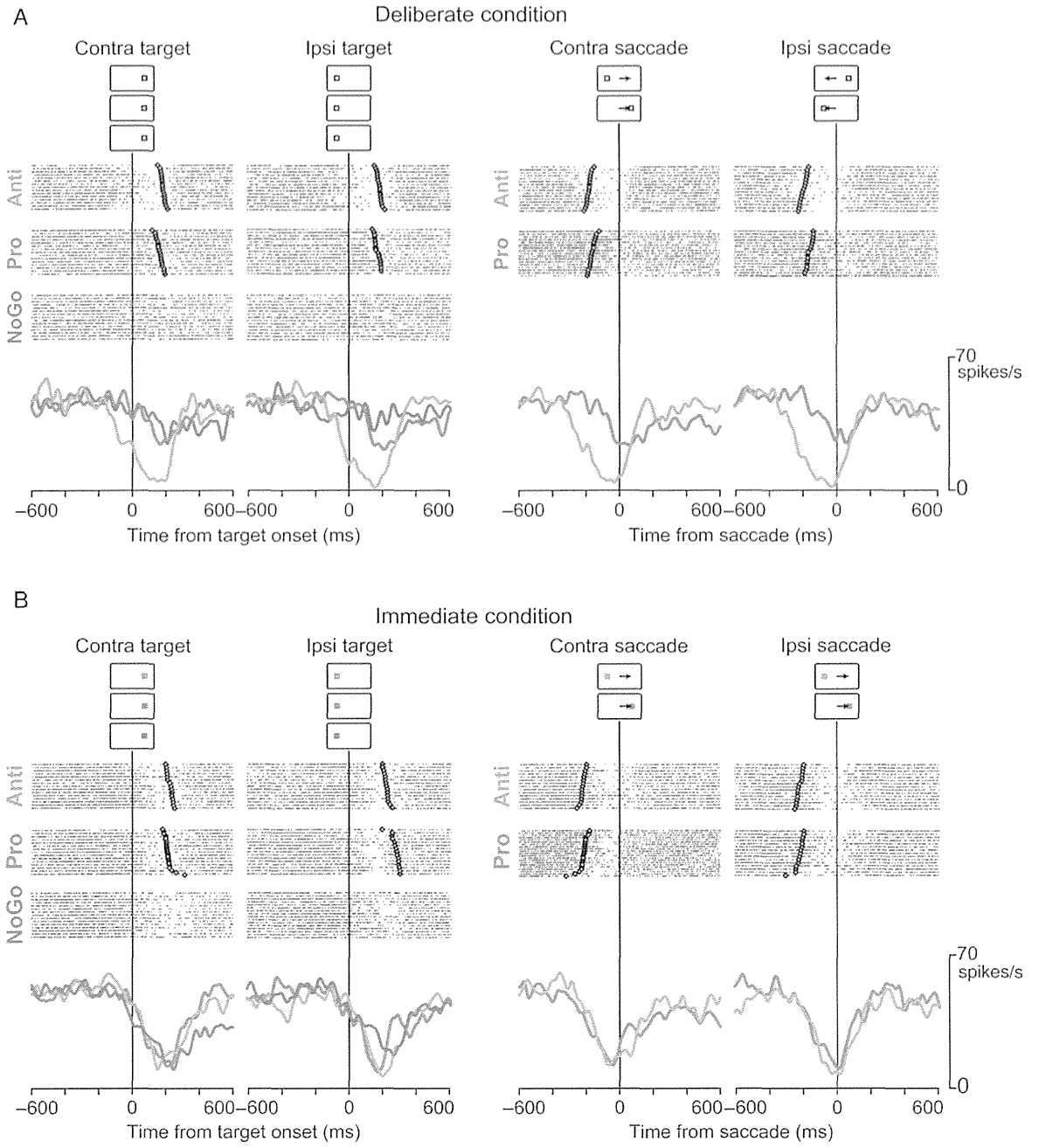

Figure 6. Comparison of the responses between paradigms for a representative decrease-type neuron. (A) Deliberate condition. (B) Immediate condition. Conventions of figures are the same as in Figure 3.

differential activity under the Immediate condition (2-way ANOVA, $P < 0.05$, followed by Scheffé's test, $P < 0.05$, Fig. 7C,G, red dots). In the population as a whole, neuronal activity in the NoGo trials was less than that during antisaccades under the Deliberate condition (paired t test, $P < 10^{-3}$ and 10^{-4} for the contralateral and ipsilateral targets, respectively). Meanwhile, neuronal activity was comparable between the trials under the Immediate condition ($P = 0.32$ and 0.29 for the contralateral and ipsilateral targets, respectively). This suggests that the decrease-type neurons might play a role in "selective" saccade suppression (Fig. 1C). As seen in the increase-type neurons, the decrease-type neurons also altered activity just before the target onset, especially in the antisaccade trials under the Deliberate condition (Fig. 7A). However, neuronal activity during stable fixation (500–1000 ms before target onset) did not vary across tasks and conditions (2-way ANOVA, $P = 0.48$).

As seen in the example neuron in Figure 6, the decrease-type neurons reduced their firing rate even during prosaccades, but the firing modulation during prosaccades was less than that during antisaccades, at least under the Deliberate condition. For multiple neurons, Figure 7B,F show the time courses of population activities during saccades. Consistent with our previous study (Yoshida and Tanaka 2009a), the firing modulation during antisaccades was greater than that during prosaccades under the

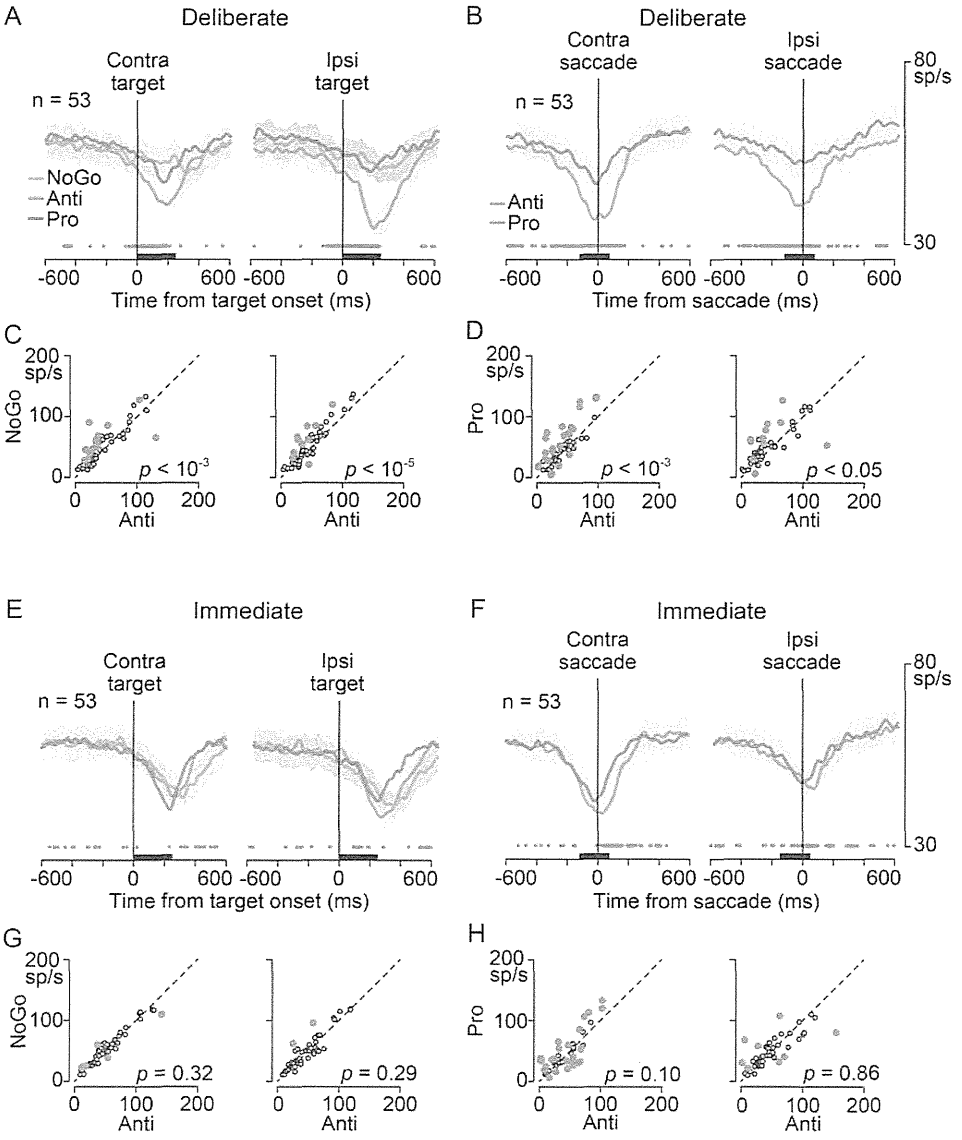

Figure 7. Quantitative analyses of the decrease-type neurons. (*A–D*) Data for the Deliberate condition. (*E–H*) Data for the Immediate condition. Conventions of figures are the same as in Figure 4. Note that the neuronal modulation during the NoGo trials was virtually absent in the Deliberate condition (A), while that in the Immediate condition was comparable with the firing modulation during antisaccades (E).

Deliberate condition (Fig. 7*B*). However, there was no significant difference in the magnitude of neuronal modulation between pro- and antisaccades under the Immediate condition (Fig. 7*F*). When the firing rates of individual decrease-type neurons were measured around the times of saccades (a 150-ms interval starting from 100 ms prior to saccades, Fig. 7*B,F*, black bars), 25 (47%, contraversive saccades) and 11 (21%, ipsiversive saccades) neurons displayed differential activity between the tasks under the Deliberate condition, and 27 (51%, contra) and 8 (15%, ipsi) neurons showed differential activity under the Immediate condition (unpaired *t* test, $P < 0.05$, Fig. 7*D,H*, red symbols). In the whole population, the magnitude of firing modulation during antisaccades was greater than that during prosaccades in the Deliberate condition (paired *t* test, $P < 10^{-3}$ and 0.05 for contraversive and ipsiversive saccades, respectively), while the neuronal modulation was comparable between the trials in the Immediate condition ($P = 0.10$ and 0.86 for contraversive and ipsiversive saccades, respectively). In contrast to the increase-type neurons (Fig. 5), we failed to find any significant correlation between neuronal activity and saccade latency in any condition, suggesting that the decrease-type neurons might not signal saccade motor commands.

If the decrease-type neurons were involved in saccade suppression, neuronal modulation during erroneous NoGo trials might be reduced as compared with that during correct trials. For a subset of neurons that could be examined during erroneous NoGo trials with targeting saccades under the Immediate condition, the neuronal activities (measured during 250 ms of target onset) averaged 52.8 ± 4.4 (SD, $n = 15$) and 64.4 ± 5.2 ($n = 12$) spikes/s for the contralateral and ipsilateral target, respectively. These values did not differ from those during correct trials (51.9 ± 4.1 and 62.2 ± 4.0 spikes/s, paired *t* test, $P > 0.05$). We

obtained similar results under the Deliberate condition (12 and 10 neurons for contralateral and ipsilateral targets, respectively), likely because the number of error trials in the NoGo trials was too small to detect a significant difference.

Discussion

We found 2 types of GPe neurons that modulated their activity associated with saccades. Similar to our previous study in other animals (Yoshida and Tanaka 2009a), the recording sites were confined to the anterior part of the dorsomedial aspect of the GPe, close to the anterior commissure. According to anatomical studies, our recording sites appear to be within the so-called associative territory, which receives signals from the dorsolateral and medial prefrontal cortices via the dorsal caudate nucleus and/or the ventral STN (Francois et al. 1994; Middleton and Strick 1994; Shink et al. 1996; for review, see Parent and Hazrati 1995b). This part of the GPe is considered to be involved in cognitive processes rather than simple motor executions (Grabli et al. 2004; Saga et al. 2013).

Absence of Confounding Effects of Visual Contrast and Task Difficulty on Neuronal Activity

Most neurons in the GPe exhibited differential activity between the tasks. For example, the magnitude of firing modulation of the increase-type neurons was greatest during antisaccades and was smallest during NoGo trials (Fig. 4). This task-rule-dependent modulation of neuronal activity was not attributed to the difference in stimulus contrast, because the response to the target was similarly affected by the task-rule under both the Deliberate and Immediate conditions, while the target was always white under the former condition (Fig. 1A). Conversely, the neuronal activity during stable fixation (100–500 ms before target onset) under the Deliberate condition did not differ across the tasks, although the color of the fixation point was different.

Also, one might argue that the task-rule-dependent modulation of neuronal activity could reflect the general difficulty of the task. It is practically impossible to adjust difficulty across the 3 paradigms; our data suggest that the task-rule-dependent modulation was not solely due to the general difficulty of the task. For example, the decrease-type neurons exhibited a similar amount of firing modulation between the tasks under the Immediate condition (Fig. 7E). Furthermore, although all tasks under the Immediate condition must be more difficult than those under the Deliberate condition, the magnitude of firing modulation was comparable between the conditions for both types of neurons (Figs. 4 and 7). Thus, the task-rule-dependent modulation of neuronal activity was likely to reflect neuronal signals that were necessary to regulate animals' behavior, rather than the stimulus attributes or general difficulty of the task. In the subsequent sections, we will consider how these signals were generated within the basal ganglia pathways, and how GPe neuronal activity could regulate voluntary movements.

Origin of Saccade Signals in the GPe

The GPe has been viewed as part of the indirect pathway, receiving signals from the striatum and sending inhibitory output to the STN (Fig. 8, the second column). Considering that the striatal neurons display a relatively lower baseline firing rate (Buser et al. 1974; Hikosaka et al. 1989) and send GABAergic projections to the GPe, neurons in the GPe would be expected to exhibit decreased activity during movements, just like our decrease-type neurons. However, we also found many neurons exhibiting increased activity during antisaccades, and in fact, more than half of the task-related neurons showed increased activity. These results are consistent with previous studies of somatic movements (for review, see Goldberg and Bergman 2011).

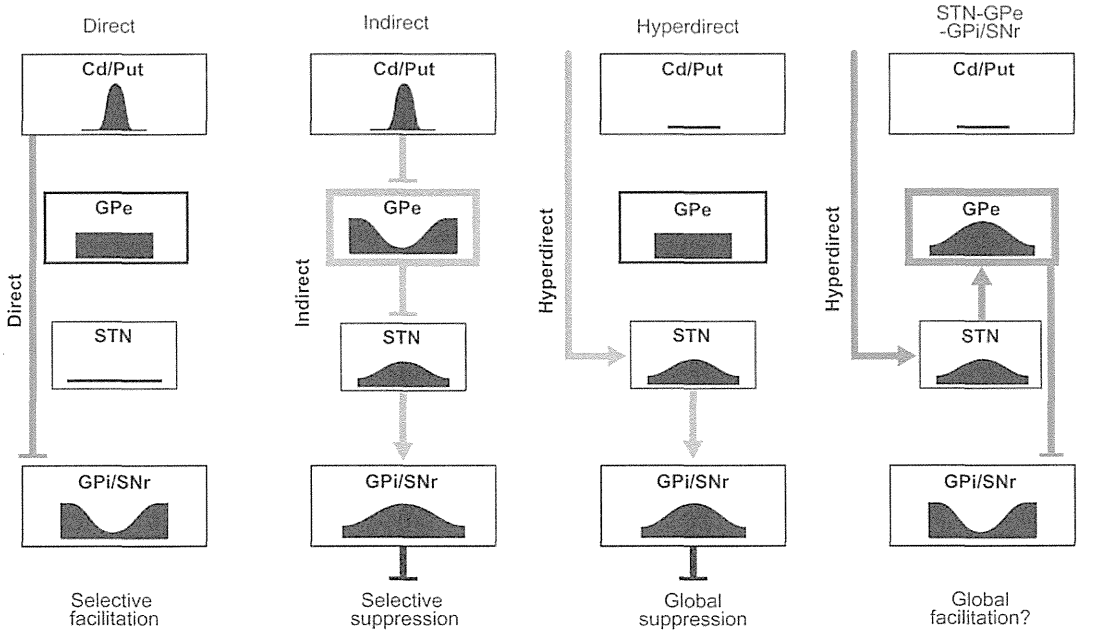

Figure 8. Diagrams showing how the signals in the GPe could facilitate antisaccades or suppress reflexive saccades. Black symbol in each rectangle indicates the direction of firing modulation during saccades. The decrease-type GPe neurons could receive direct inputs from the caudate nucleus (Cd) through the indirect pathway, while the increase-type GPe neurons might receive signals through the cortico-STN-GPe pathways. The indirect and hyperdirect pathways may suppress reflexive saccades, while the direct and cortico-STN-GPe pathways might facilitate voluntary saccades: these pathways might be involved in selective and global facilitations, respectively. Cd, caudate nucleus; GPi, internal segment of the globus pallidus; SNr, substantia nigra pars reticulata; STN. Subthalamic nucleus.

How do neurons in the GPe generate increased activity associated with saccades? Because the GPe receives projections from multiple nuclei in the basal ganglia, there are several possible mechanisms activating GPe neurons. For example, a transient suppression of inhibitory signals from the striatum, a release of lateral inhibition within the GPe, or feedback through the striatal-GPe-STN-GPe pathways might underlie the increased activity. However, previous studies demonstrated that excitation of GPe neurons following cortical stimulation was mediated by the cortico-STN-GPe pathways (Nambu et al. 2000; Kita et al. 2004). Furthermore, a recent study has shown that most increasing signals in GPe neurons during voluntary movements are attributed to glutamatergic inputs, while most of decreasing signals reflect GABAergic projections (Kaneko et al. 2014). Anatomical data also suggest the possibility that the increase-type neurons might receive glutamatergic inputs from the STN (Shink et al. 1996). The STN receives direct projections from the cerebral cortex (Inase et al. 1999; Nambu et al. 1996; Kelly and Strick 2004) and composes the "hyperdirect" pathway that elevates neuronal activity in the substantia nigra pars reticulata (SNr) and the internal segment of the GP (GPi) (Smith et al. 1990; Parent and Hazrati 1995a; Figure 8, the third column). In addition to the hyperdirect pathway, which ultimately suppresses neuronal activity in the superior colliculus (SC) or the thalamus (Nambu et al. 2002), GPe neurons also have direct access to the SNr and GPi (Smith et al. 1990; Sato et al. 2000), which could facilitate signals in the SC and thalamus via the disinhibition mechanisms (Fig. 8, right column). Thus, the different types of signals in the GPe might come from 2 different sources.

Possible Roles of Two Different Pathways Through the GPe

What then are the roles of the pathways mediated by the 2 different types of GPe neurons? Previous studies suggest that each basal ganglia pathway is assigned to the regulation of a different aspect of movement. For example, the direct pathway in the basal ganglia is thought to be involved in the generation of purposeful actions (for review, see Hikosaka et al. 2000). Neurons in the caudate nucleus, the SNr and the SC exhibit greater firing modulation during memory-guided saccades compared with visually guided saccades (Hikosaka and Wurtz 1983a,b; for review, see Shires et al. 2010). The enhancement of neuronal modulation in the direct pathway during antisaccades has also been reported (Ford and Everling 2009; Watanabe and Munoz 2009), and these signals seem to have a causal role in the generation of antisaccades (Watanabe and Munoz 2010b). Based on neuronal activity in the caudate nucleus, Watanabe and Munoz (2009, 2010a) have proposed that neurons with a preference for contraversive saccades may facilitate antisaccades through the direct pathway, while those with an ipsilateral preference may suppress reflexive saccades via the indirect pathway. According to this hypothesis, the decrease-type neurons in the GPe found in the present study might receive volitional signals from the caudate nucleus and suppress contraversive reflexive saccades. On the other hand, we found a significant negative correlation between neuronal activity of the increase-type neurons and antisaccade latency under both conditions (Fig. 5), suggesting that these neurons might play a role in facilitating saccades, in a similar manner to neurons in the caudate nucleus that have a contralateral preference (Hikosaka et al. 1989; Lau and Glimcher 2007). Unfortunately, however, our study could not elucidate how these GPe neurons facilitate antisaccades in cooperation with the volitional neurons in the caudate nucleus. One possibility is that neurons in the SNr and GPi might be suppressed through both the direct and the cortico-STN-GPe-SNr/GPi pathways (Fig. 8, right column), causing disinhibition in the downstream structures when the 2 parallel pathways transmit signals simultaneously.

In relation to this, Isoda and Hikosaka (2008) found 2 types of neurons in the ventral STN as monkeys switched from automatic to volitional saccades. One type of neuron exhibited a transient activity during behavioral switching, while the other was active as the animals suppressed automatic saccades (no-go neuron). Our increase-type neurons in the GPe might be relevant to the former neurons, both of which are likely to facilitate volitional saccades (Isoda and Hikosaka 2008). Consistent with this, many increase-type neurons also exhibited some activity during prosaccades, although the magnitude of firing modulation was smaller than that during antisaccades (Fig. 4). The signals carried by the increase-type GPe neurons might facilitate saccades in general, while the contribution of these signals appears to be dominant for antisaccades. In contrast, the decrease-type neurons in the GPe and the no-go neurons in the STN might play a role in suppressing reflexive saccades. These hypotheses could be tested in future studies by pharmacological manipulation of signals in the different GPe pathways.

Global and Selective Suppression of Movements

To elucidate how signals in the GPe suppress unwanted movements, we introduced the NoGo trial under 2 different conditions. In the Deliberate condition, the animals might simply ignore any visual stimulus during the NoGo trials, whereas in the Immediate condition, they had to pay attention to the target to understand the task being performed. Thus, the suppression of reflexive saccades must be more selective under the Immediate condition compared with the Deliberate condition (Fig. 1C). Our data showed that the magnitude of firing modulation in the decrease-type neurons during NoGo trials was comparable with that during antisaccades under the Immediate condition, whereas the same neurons exhibited only a slight change in activity in the NoGo trials under the Deliberate condition. These results suggest that the indirect pathway mediated by the decrease-type neurons in the GPe might be related to the selective inhibition of unwanted actions. Our findings are in line with the recent proposal that the indirect and hyperdirect pathways mediate signals for selective and global suppression, respectively (Majid et al. 2013; for review, see Aron 2011). To further confirm this hypothesis, future studies need to examine causal roles of each type of GPe signal in the generation of antisaccades.

In conclusion, we found 2 types of neurons in the GPe that exhibited different firing modulation during NoGo and antisaccade trials. We suggest that the increase-type neurons are involved in the process of saccade facilitation, while the decrease-type neurons are relevant to the selective suppression of reflexive saccades. The increase-type neurons could be involved in the cortico-STN-GPe-SNr/GPi pathway, which might operate in parallel with the direct, indirect and hyperdirect pathways in the basal ganglia.

Funding

This work was supported by grants from the Ministry of Education, Culture, Sports, Science and Technology of Japan, the Ministry of Health, Labour and Welfare of Japan, the Japan Society for the Promotion of Science, the Smoking Research Foundation and the Takeda Science Foundation. A.Y. was supported by the Graduate Research Fellowship for Young Scientists from the Japan Society for the Promotion of Science. Animals were provided by the National Bio-Resource Project.

Notes

We are grateful to T. Mori and A. Hironaka for the animal care, M. Suzuki for administrative help, and all laboratory members for comments and discussions. *Conflict of Interest*: None declared.

References

Abegg M, Sharma N, Barton JJ. 2012. Antisaccades generate two types of saccadic inhibition. Biol Psychol. 89:191–194.

Albin RL, Young AB, Penney JB. 1989. The functional anatomy of basal ganglia disorders. Trends Neurosci. 12:366–375.

Aron AR. 2011. From reactive to proactive and selective control: developing a richer model for stopping inappropriate responses. Biol Psychiatry. 69:e55–e68.

Brotchie P, Iansek R, Horne MK. 1991. Motor function of the monkey globus pallidus. 1. Neuronal discharge and parameters of movement. Brain. 114:1667–1683.

Buser P, Pouderoux G, Mereaux J. 1974. Single unit recording in the caudate nucleus during sessions with elaborate movements in the awake monkey. Brain Res. 71:337–344.

Chan CS, Surmeier DJ, Yung WH. 2005. Striatal information signaling and integration in globus pallidus: timing matters. Neurosignals. 14:281–289.

DeLong MR. 1990. Primate models of movement disorders of basal ganglia origin. Trends Neurosci. 13:281–285.

Ford KA, Everling S. 2009. Neural activity in primate caudate nucleus associated with pro- and antisaccades. J Neurophysiol. 102:2334–2341.

Francois C, Grabli D, McCairn K, Jan C, Karachi C, Hirsch EC, Feger J, Tremblay L. 2004. Behavioural disorders induced by external globus pallidus dysfunction in primates II. Anatomical study. Brain. 127:2055–2070.

Francois C, Yelnik J, Percheron G, Fenelon G. 1994. Topographic distribution of the axonal endings from the sensorimotor and associative striatum in the macaque pallidum and substantia nigra. Exp Brain Res. 102:305–318.

Goldberg JA, Bergman H. 2011. Computational physiology of the neural networks of the primate globus pallidus: function and dysfunction. Neuroscience. 198:171–192.

Grabli D, McCairn K, Hirsch EC, Agid Y, Feger J, Francois C, Tremblay L. 2004. Behavioural disorders induced by external globus pallidus dysfunction in primates I. Behavioural study. Brain. 127:2039–2054.

Haber SN, Lynd-Balta E, Mitchell SJ. 1993. The organization of the descending ventral pallidal projections in the monkey. J Comp Neurol. 329:111–128.

Hikosaka O, Sakamoto M, Usui S. 1989. Functional properties of monkey caudate neurons. I. Activities related to saccadic eye movements. J Neurophysiol. 61:780–798.

Hikosaka O, Takikawa Y, Kawagoe R. 2000. Role of the basal ganglia in the control of purposive saccadic eye movements. Physiol Rev. 80:953–978.

Hikosaka O, Wurtz RH. 1983a. Visual and oculomotor functions of monkey substantia nigra pars reticulata. I. Relation of visual and auditory responses to saccades. J Neurophysiol. 49:1230–1253.

Hikosaka O, Wurtz RH. 1983b. Visual and oculomotor functions of monkey substantia nigra pars reticulata. III. Memory-contingent visual and saccade responses. J Neurophysiol. 49:1268–1284.

Inase M, Tokuno H, Nambu A, Akazawa T, Takada M. 1999. Corticostriatal and corticosubthalamic input zones from the presupplementary motor area in the macaque monkey: comparison with the input zones from the supplementary motor area. Brain Res. 833:191–201.

Isoda M, Hikosaka O. 2008. Role for subthalamic nucleus neurons in switching from automatic to controlled eye movement. J Neurosci. 28:7209–7218.

Kaneko N, Hatanaka N, Takara S, Takada M, Nambu A. 2014. Glutamatergic and GABAergic control of monkey pallidal activity during performance of a motor task. Japan Neurosci Soc Abstr. 37:1.141.

Kato M, Hikosaka O. 1995. Functional of the indirect pathway in the basal ganglia oculomotor system: visuo-oculomotor activities of external pallidum neurons. In: Segawa M, Nomura Y, editors. Age-related dopamine-deficient disorders. Basal: Karger. pp. 178–187.

Kelly RM, Strick PL. 2004. Macro-architecture of basal ganglia loops with the cerebral cortex: use of rabies virus to reveal multisynaptic circuits. Prog Brain Res. 143:449–459.

Kita H, Nambu A, Kaneda K, Tachibana Y, Takada M. 2004. Role of ionotropic glutamatergic and GABAergic inputs on the firing activity of neurons in the external pallidum in awake monkeys. J Neurophysiol. 92:3069–3084.

Lau B, Glimcher PW. 2007. Action and outcome encoding in the primate caudate nucleus. J Neurosci. 27:14502–14514.

Majid DS, Cai W, Corey-Bloom J, Aron AR. 2013. Proactive selective response suppression is implemented via the basal ganglia. J Neurosci. 33:13259–13269.

Middleton FA, Strick PL. 1994. Anatomical evidence for cerebellar and basal ganglia involvement in higher cognitive function. Science. 266:458–461.

Mitchell SJ, Richardson RT, Baker FH, DeLong MR. 1987. The primate globus pallidus: neuronal activity related to direction of movement. Exp Brain Res. 68:491–505.

Munoz DP, Everling S. 2004. Look away: the anti-saccade task and the voluntary control of eye movement. Nat Rev Neurosci. 5:218–228.

Nambu A, Takada M, Inase M, Tokuno H. 1996. Dual somatotopical representations in the primate subthalamic nucleus: evidence for ordered but reversed body-map transformations from the primary motor cortex and the supplementary motor area. J Neurosci. 16:2671–2683.

Nambu A, Tokuno M, Hamada I, Kita H, Imanishi M, Akazawa T, Ikeuchi Y, Hasegawa N. 2000. Excitatory cortical inputs to pallidal neurons via the subthalamic nucleus in the monkey. J Neurophysiol. 84:289–300.

Nambu A, Tokuno H, Takada M. 2002. Functional significance of the cortico-subthalamo-pallidal 'hyperdirect' pathway. Neurosci Res. 43:111–117.

Parent A, Hazrati LN. 1995a. Functional anatomy of the basal ganglia. I. The cortico-basal ganglia-thalamo-cortical loop. Brain Res Brain Res Rev. 20:91–127.

Parent A, Hazrati LN. 1995b. Functional anatomy of the basal ganglia. II. The place of subthalamic nucleus and external pallidum in basal ganglia circuitry. Brain Res Brain Res Rev. 20:128–154.

Saga Y, Hashimoto M, Tremblay L, Tanji J, Hoshi E. 2013. Representation of spatial- and object-specific behavioral goals in the dorsal globus pallidus of monkeys during reaching movement. J Neurosci. 33:16360–16371.

Sato F, Lavallee P, Levesque M, Parent A. 2000. Single-axon tracing study of neurons of the external segment of the globus pallidus in primate. J Comp Neurol. 417:17–31.

Shin S, Sommer MA. 2010. Activity of neurons in monkey globus pallidus during oculomotor behavior compared with that in substantia nigra pars reticulata. J Neurophysiol. 103:1874–1887.

Shink E, Bevan MD, Bolam JP, Smith Y. 1996. The subthalamic nucleus and the external pallidum: two tightly interconnected structures that control the output of the basal ganglia in the monkey. Neuroscience. 73:335–357.

Shires J, Joshi S, Basso MA. 2010. Shedding new light on the role of the basal ganglia-superior colliculus pathway in eye movements. Curr Opin Neurobiol. 20:717–725.

Smith Y, Hazrati LN, Parent A. 1990. Efferent projections of the subthalamic nucleus in the squirrel monkey as studied by the PHA-L anterograde tracing method. J Comp Neurol. 294:306–323.

Tanaka M. 2005. Involvement of the central thalamus in the control of smooth pursuit eye movements. J Neurosci. 25:5866–5876.

Turner RS, Anderson ME. 1997. Pallidal discharge related to the kinematics of reaching movements in two dimensions. J Neurophysiol. 77:1051–1074.

Watanabe M, Munoz DP. 2009. Neural correlates of conflict resolution between automatic and volitional actions by basal ganglia. Eur J Neurosci. 30:2165–2176.

Watanabe M, Munoz DP. 2010a. Presetting basal ganglia for volitional actions. J Neurosci. 30:10144–10157.

Watanabe M, Munoz DP. 2010b. Saccade suppression by electrical microstimulation in monkey caudate nucleus. J Neurosci. 30:2700–2709.

Wichmann T, DeLong MR, Guridi J, Obeso JA. 2011. Milestones in research on the pathophysiology of Parkinson's disease. Mov Disord. 26:1032–1041.

Yoshida A, Tanaka M. 2009a. Enhanced modulation of neuronal activity during antisaccades in the primate globus pallidus. Cereb Cortex. 19:206–217.

Yoshida A, Tanaka M. 2009b. Neuronal activity in the primate globus pallidus during smooth pursuit eye movements. Neuroreport. 20:121–125.

Systems/Circuits

Different Neuronal Computations of Spatial Working Memory for Multiple Locations within versus across Visual Hemifields

Ayano Matsushima and Masaki Tanaka
Department of Physiology, Hokkaido University School of Medicine, Sapporo 060-8638, Japan

Spatial working memory is one of the most studied cognitive functions, serving as a model system to decipher computational principles of the brain. Although neuronal mechanisms for remembering a single location have been well elucidated, little is known about memory for multiple locations. Here, we examined the activities of prefrontal neurons during monkeys remembered positions of one or two visual cue(s). When the two cues were presented across the left and right visual fields, neurons exhibited a comparable response to the activity for the preferred cue presented alone. When the two cues were presented within the same hemifield, neurons exhibited an intermediate response between those to the individual cues. Subsequent computer simulations predicted a lower signal-to-noise ratio in the latter condition, which was further verified by behavioral experiments. Considering the separation of contralateral and ipsilateral visual processing, the lateral inhibition in local circuits might implicitly determine different neuronal computations and memory capacities for bilateral and unilateral displays.

Key words: memory capacity; prefrontal cortex; primate; single-unit recording; working memory

Introduction

Working memory, the ability to selectively maintain task-relevant information for subsequent behavior and thoughts, constitutes a fundamental building block of cognition (Goldman-Rakic, 1995). Exploration of its neuronal correlates has been remarkably advanced through the development of delayed-response paradigms (Fuster and Alexander, 1971; Kubota and Niki, 1971), in particular, the memory-guided saccade task (Hikosaka and Wurtz, 1983). In the cortical network that includes the prefrontal cortex (PFC) (Bruce and Goldberg, 1985; Gnadt and Andersen, 1988; Funahashi et al., 1989), many neurons show sustained, enhanced activity after a brief presentation of a visual cue. Because the delay-period activities are spatially tuned, the remembered location can be encoded as the preferred location of the most active neurons in the population, which is thought to be an efficient neuronal code for spatial working memory.

However, it remains unanswered how the brain maintains information about multiple locations simultaneously. Based on previous results, there are three possibilities. First, each neuron might solely signal the presence of a visual cue in the preferred location to be remembered, ignoring any other cues presented previously (Edin et al., 2009; Wei et al., 2012). Second, there might be neurons encoding multiple locations as a single packet. In line with this, when monkeys remembered the identities of two visual objects, prefrontal neurons nonlinearly combined a representation of each item to respond to a specific pair (Warden and Miller, 2007). Finally, neuronal activity might reflect the competitive interaction of multiple representations. The biased competition model of selective attention suggests that responses to individual stimuli are linearly integrated with biases toward attended objects (Desimone and Duncan, 1995; Reynolds and Heeger, 2009), which has much empirical support (Moran and Desimone, 1985; Treue and Maunsell, 1996). Because computations within individual neurons must limit the representational capacity of the whole population (Rigotti et al., 2013), it is of great importance to elucidate how each neuron encodes multiple locations.

In the present study, we examined the activities of prefrontal neurons while monkeys remembered the location of one or two visual cue(s). Our data show that each neuron represents multiple locations differently depending on whether the stimuli were presented across or within visual hemifield(s). We suggest that the inherent, anatomical separation of contralateral and ipsilateral information might differentiate neuronal computations for bilateral and unilateral displays, imposing physiological constraints on the memory capacity.

Received Jan. 21, 2014; revised Feb. 17, 2014; accepted March 19, 2014.

Author contributions: A.M. and M.T. designed research; A.M. performed research; A.M. analyzed data; A.M. and M.T. wrote the paper.

This work was supported by the Ministry of Education, Culture, Sports, Science and Technology of Japan, the Ministry of Health, Labour and Welfare of Japan, the Japan Society for the Promotion of Science, the Smoking Research Foundation, and the Takeda Science Foundation. Animals were provided by the National Bio-Resource Project. We thank T. Mori and A. Hironaka for the animal care, M. Suzuki for administrative help, and all laboratory members for comments and discussions.

The authors declare no competing financial interests.

Correspondence should be addressed to Dr. Ayano Matsushima, Department of Neurochemistry, Graduate School of Medicine, The University of Tokyo, Tokyo, Japan. E-mail: ayano.violine@gmail.com.

DOI:10.1523/JNEUROSCI.0295-14.2014

 0270-6474/14/345621-06$15.00/0